Immunopathologia Persa
http immunopathol.com
DOI:10.34172/ipp.2023.40589

LSPR aptasensor based on gold nanoparticles for rapid detection of HIV type-1 nucleic acid

Maryam Fatemipour[1], Masoumeh Zahmatkeshan[2,3], Seyed Jalal Kiani[1], Ahmad Tavakoli[4], Farah Bokharaei-Salim[1], Behnam Khodadost[5], Seyed Ahmad Dehdast[6], Milad Sabaei[7], Vahid Pirhajati Mahabadi[8], Mohammad Reza Rezvani[9], Seyed Hamidreza Monavari[1*]

[1]Department of Virology, School of Medicine, Iran University of Medical Sciences, Tehran, Iran
[2]Cellular and Molecular Research Center, Iran University of Medical Sciences, Tehran, Iran
[3]Department of Medical Nanotechnology, Faculty of Advanced Technologies in Medicine, Iran University of Medical Sciences, Tehran, Iran
[4]Research Center of Pediatric Infectious Diseases, Institute of Immunology and Infectious Diseases, Iran University of Medical Sciences, Tehran, Iran
[5]Endocrinology and Metabolism Research Center, Hormozgan University of Medical Sciences, Bandar Abbas, Iran
[6]Department of Biochemistry, School of Medicine, Iran University of Medical Sciences (IUMS), Tehran, Iran
[7]Antimicrobial Resistance Research Center, Institute of Immunology and Infectious Diseases, Iran University of Medical Sciences, Tehran, Iran
[8]Neuroscience Research Center, Iran University of Medical Sciences (IUMS), Tehran, Iran
[9]Department of Hematology, Faculty of Allied Medicine, Iran University of Medical Sciences, Tehran, Iran

***Correspondence to**
Seyed Hamidreza Monavari, Email: hrmonavari@yahoo.com

Received 10 Sep. 2023
Accepted 15 Nov. 2023
ePublished 4 Dec. 2023

Keywords: HIV, Localized surface plasmon resonance, Aptamer, Biosensor, Rapid detection

Abstract

Introduction: Economic and dependable detection of the human immunodeficiency virus (HIV) is crucial to controlling and managing the infection, especially for almost half of the HIV-affected population (46%) unaware of their HIV status. Currently, the existing technologies' cost, expertise, and time requirements severely restrict their widespread use, particularly among populations with limited resources.
Objectives: The current study aimed to design a rapid and low-cost assay platform to detect qualitatively and quantitatively the unamplified HIV RNA using gold nanoparticles' (AuNPs') unique physicochemical and optical properties. This research is based on inducing the aggregation of AuNPs functionalized with a thiol-modified probe by a cationic agent.
Patients and Methods: In this experimental study, total RNA was extracted from 56 patients with established HIV infection and 38 healthy HIV-negative participants, followed by mixing the extracted RNA, AuNP-probes, and cationic-AuNPs. Next, the solutions' color changes were assessed visually and by UV-vis spectrophotometry. The viral load of each sample was calculated using the equation established by the standard curve.
Results: The assay could detect HIV-RNA extracted from plasma, and the results were comparable to those of reverse transcription-quantitative polymerase chain reaction (RT-qPCR). Target-AuNP-probe hybrids were stable during aggregation after adding the cationic inducer. The standard curve plot showed a relatively wide linear range. With 89.2% sensitivity and 92.1% specificity, the test had a limit of detection (LOD) of 160 IU/mL.
Conclusion: To our knowledge, this is the first study on the effect of using modified gold and cationic nanoparticles to detect non-amplified HIV nucleic acid. The assay detected HIV-RNA within 70 minutes, confirmed by color changes visible to the naked eye and measurable by recording the absorption spectrum. This technology can be extended to identify other nucleic acid targets and adapt full automation.

Citation: Fatemipour M, Zahmatkeshan M, Kiani SJ, Tavakoli A, Bokharaei-Salim F, Khodadost B, Dehdast SA, Sabaei M, Pirhajati Mahabadi V, Rezvani MR, Monavari SH. LSPR aptasensor based on gold nanoparticles for rapid detection of HIV type-1 nucleic acid. Immunopathol Persa. 2024;10(1):e40589. DOI:10.34172/ipp.2023.40589.

Introduction

The human immunodeficiency virus type-1 (HIV-1) became a major global concern with the introduction of the deadly acquired immunodeficiency syndrome (AIDS) (1). Since the start of the epidemic, around 60 million individuals have been infected with HIV. Almost 60% of those infected with HIV have not received antiviral treatment, and about half (46%) are unaware of their disease status and are considered asymptomatic carriers. Therefore, the availability of convenient and accurate methods to detect HIV-related biomarkers is very important in the early diagnosis and treatment of patients with AIDS (2). Typically, tests for detecting anti-HIV antibodies are performed on serum or plasma for initial diagnosis and screening. The significant feature of the early stages of HIV infection is the lack of detectable antibodies and the transient high viral load (3).

However, antibody-based techniques are not much efficient in detecting HIV-1 in the

Key point

In this study, an RNA sensor based on oligonucleotide target-specific gold nanoparticles was developed. The aptasensor demonstrated superior analytical and clinical performance for HIV diagnosis in clinical samples.

early stages when antibodies have not yet been developed by the immune system (window period) (4). Also, these techniques cannot be performed on newborns from mothers infected with HIV up to 12 months or more, due to the presence of antibodies transmitted from mother to baby (5). The HIV-RNA and P24 antigenic protein are other virological markers that can be used to determine the infection status. The P24 antigenic protein is usually detectable in the serum only 3 months after the initial infection. It reappears in the serum years later, when the infection progresses to AIDS. To date, methods for direct detection of viral nucleic acid, e.g., polymerase chain reaction (PCR), have been considered the best way for early detection of infection. Despite the high accuracy of these tests, they are expensive, time-consuming, slow to give results, and require skilled personnel and specialized laboratory equipment. Therefore, alternative approaches and practical detection methods are needed to detect viral nucleic acid (6, 7).

Regarding the mentioned points, researchers have recently focused on developing biosensor systems for biomarker detection, especially biosensors based on gold nanoparticles (AuNPs). AuNPs-based calorimetric biosensors have been employed as powerful measurement tools for the early detection of analytes because of their special properties, including unique spectral absorption properties, high ability to bind to biological molecules, non-toxicity, and large surface area to volume ratio (8).

Gold nanoparticles have distinctive Localized Surface Plasmon Resonance (LSPR) behavior, leading to their intense red color and high attenuation coefficient. This behavior is among the most important characteristics distinguishing gold from other metals (9). The resonant frequency of gold nanoparticles for conduction band electrons is located in the visible part of the electromagnetic spectrum (10).

Unlike other metal nanoparticles, gold nanoparticles have optical properties that are easily visible to the naked eye, without complex instruments (11). These nanoparticles serve as signal-transmitting elements in cross-linking (CL) or non-cross-linking (NCL) techniques to identify nucleic acid sequences. The CL method was initially developed for nucleic acid detection using modified AuNPs (12). In this method, two different types of SH-ssDNA probes are conjugated on the AuNPs surface, and the target DNA acts as a cross-linker between two functionalized AuNPs.

In the earliest report of the NCL method for DNA detection, a single-strand thiol-modified probe was used for AuNPs functionalization (13). Here, the aggregation of nanoparticles was induced by a moderate ionic agent. In metal nanoparticle-based colorimetric investigations, NaCl cationic salt is often used as an aggregation inducer (14).

Objectives

In the present research, for the first time, we developed a simple workflow colorimetric assay to detect HIV-RNA using AuNPs functionalized with a single-strand thiolated-oligonucleotide (AuNP-probes). In this system, the aggregation of nanoparticles is induced by cationic nanoparticles (Figure 1). The proposed nano-assay detects the HIV-RNA by color changes visible to the naked eye. This assay can especially meet the healthcare needs of regions with limited resources and extended for identifying other nucleic acid targets and adapting full automation.

Patients and Methods

Materials and equipment

Hydrogen tetrachloroaurate (III) trihydrate, TCEP-HCL (Tris 2-carboxyethyl phosphine-hydrochloride), Sodium dodecyl sulfate, Cetyl trimethylammonium bromide, dibasic and monobasic phosphate, and other analytical-grade chemical compounds were purchased from Sigma-Aldrich, Germany. Also, the QIAamp DSP Virus kit and the Artus HIV-1 RG RT-PCR were purchased from Qiagen GmbH, Hilden, Germany. UV-vis spectra and oligonucleotide concentrations were recorded using Eppendorf Bio-spectrophotometer basic and Nanodrop (Thermo Fisher ND 1000, USA), respectively. The size and zeta potential of AuNPs were determined using a Zetasizer Nano ZS (Malvern, England). A high-resolution transmission electron microscope (TEM, Philips CM30 200 KV TEM) was used to image nanoparticles.

Plasma samples collection

In this experimental study, samples were collected from 56 patients with established HIV infection referred to the laboratory of HIV Center associated with the Iran University of Medical Sciences and 38 healthy HIV-negative participants. All samples were subjected to rapid Hepatitis C virus and Hepatitis B virus antibody testing. HIV-positive cases co-infected with Hepatitis B virus (HBV) or hepatitis C virus (HCV) were excluded from the study. The inclusion criteria were positive anti-HIV antibodies along with positive plasma HIV RNA. The HIV-positive patients had no acute diseases or infections such as cytomegalovirus (CMV), mycobacterium tuberculosis, and Kaposi's sarcoma cancer. Besides, they had no known autoimmune diseases, genetic disorders, or medication toxicity concurrently. Each individual provided a peripheral blood sample of around 6 ml. The sample was then placed in a sterile vacutainer tube containing EDTA. After separation, the plasma was kept at

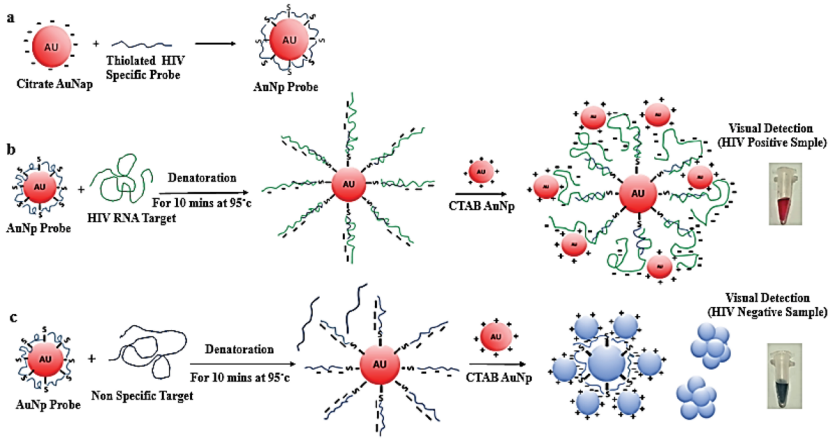

Figure 1. A schematic view of HIV RNA detection using colorimetric nano-assay based on modified AuNPs: (a) Citrate AuNPs were first functionalized with thiolated HIV-specific oligonucleotide probes. (b) The HIV viral RNA was mixed with nanoprobes and heated for 10 minutes at 95℃ for RNA denaturation. The HIV RNA was hybridized to its complementary sequence in the nanoprobe. After cooling the solution at room temperature, cationic CTAB-AuNPs (Cetyl trimethylammonium bromide-AuNPs) were added to induce the aggregation of gold nanoparticles. In the presence of target HIV-RNA, the dispersion of cationic CTAB-AuNPs onto the folded HIV RNA prevents the aggregation of AuNPs. As a result, the color of the solution remains red. (c) In the lack of a complementary HIV-RNA, CTAB-AuNPs were bound to the backbone of the phosphate probe. Therefore, the inter-particle distance between the AuNP-probes and the CTAB-AuNPs decreased, leading to aggregation and a color change from red to blue.

-70°C. RNA extraction and real-time PCR were performed on all samples to identify HIV RNA.

Synthesis and characterization of different AuNPs

Citrate-capped colloidal AuNPs with diameters of 18 nm were synthesized using the *modified* sodium citrate reduction methods *(15)*. Positive surface charge functionalization of AuNPs was then performed using capped CTAB. Gold nanoprobes were prepared via aptamer functionalization on the NPs surface using the salt aging method (16). Briefly, the disulfide bonds of thiolated probes were reduced via the TCEP-HCL solution, followed by adding the reduced probes (10 µM, 13 µL) to AuNPs solution (25 µM, 400 µL). The HIV probe consisted of 28 nucleotides that were complementary to the sequence before the start of the codon of the HIV genome's Gag region, including nucleotides 318-335 (i.e., conserved region in all genotypes and subtypes of HIV-1). The probe (5′- Thiol-C6-AAA AAA AAA ACT CTC TCC TTC TAG CCT C -3′) was alkane-thiol modified at its 5-terminus. The conventional seed-mediated growth approach was used for CTAB-AuNPs synthesis (17). Transmission electron microscopy (TEM), dynamic light scattering (DLS), and UV/visible spectrophotometry were used to examine the shape, size, charge, and spectroscopic characteristics of the produced citrate-AuNPs, AuNP-probes, and CTAB-AuNPs.

Nano-assay optimization

Various concentrations of the TCEP-treated thiolated RNA (0.5, 1, 10, 50, 100, and 150 µM) were combined with different concentrations of the citrate-AuNPs solution (150, 100, 50, 25, and 10µM) and incubated for 16 hours at 25°C before the salt aging stages to optimize the probe concentration.

The CTAB-AuNPs concentration was optimized by mixing CTAB-AuNPs solutions in various concentrations (0.1-1.1 µM) and volumes (1-1.7 µL) with 13 µL AuNP-probe solution and incubated for 5 min at 25 °C. This solution contained 6 µL nanoprobe and 7 µL Tris-Hcl buffer. The lowest amount of CTAB-AuNP that triggered nanoparticle aggregation and the resultant color change in the solution was considered the optimal volume for the assay. UV-vis spectrophotometry was used to assess each concentration's absorbance at 525 nm.

AuNPs colorimetric assay for RNA detection

The nano-assay was performed by adding 6 µL of AuNP probe to 7 µL of the extracted RNA sample. The mixture was incubated at 95 °C for 10 minutes to denature the RNA. Once the solution cooled to room temperature for 20 minutes, 1.3 µL of CTAB-AuNP was added and carefully mixed. Solutions' color changes were assessed visually and by UV-vis spectrophotometry, and the absorption spectra were recorded in the wavelength range of 400 to 750 nm.

Quantification of HIV-RNA in plasma using nano-assay

HIV RNA load was determined using the Artus HIV-1 RG RT-PCR kit according to the kit's manual. Based on the kit instruction, 1 IU/mL corresponds to 0.50 copies/mL for the detection of HIV-1 RNA. Serial dilutions were then prepared from a positive HIV sample with a certain concentration, and a nano-assay was conducted on all dilutions (i.e., 300-50 000 IU/mL). Spectral absorption for each dilution was measured by UV-vis spectrophotometry at two wavelengths: λ525 for non-aggregated nanoprobes and λ650 for aggregated nanoprobes. All absorption tests were performed in triplicate. Afterward, the standard curve was drawn by setting the λ525 to λ650 absorption ratio values (A525/A650) on the Y axis against the HIV

RNA log concentration values on the X axis.

HIV RNA using the nano-assay, the viral load of all HIV RNA samples was calculated (1-2 000 000 IU/mL) using the corresponding A525/A650 ratios obtained from the nano-assay and the equation established by the standard curve. The receiver operating characteristic (ROC) curve was drawn using SPSS software (IBM SPSS Statistics 23). The analyses were performed using nano-assay results on plasma samples of HIV-infected patients and healthy individuals. Next, the ROC curve was used to determine the cut-off, specificity, and sensitivity of the nano-assay (Table S2). The limit of detection (LOD) was determined by preparing a serial dilution (5-fold dilution factor, up to 1 IU/mL) of HIV RNA. Afterward, it was analyzed using a standard curve after performing a nano-assay for each concentration (in triplicate). The LOD of the nano-assay was determined by identifying the lowest concentration of HIV RNA, in which the initiation of nanoparticle aggregation was observed at least in two out of three replicates.

TEM analysis of different AuNPs and positive and negative HIV samples

In this study, the size and morphology of citrate-AuNPs, AuNP-probes, and CTAB-AuNPs were checked by performing TEM analysis. Moreover, the changes in the shape and size of nanoparticles before and after the nano-assay were compared by performing the TEM imaging for two positive and negative HIV samples.

HIV RNA extraction and real-time PCR

The RNA was extracted using a QIAamp DSP virus kit as directed by the manufacturer. Additionally, RT-PCR was carried out using the Artus HIV-1 RG RT-PCR Qiagen GmbH kit following the kit's instructions to ascertain the viral load.

Statistical analysis

The *t* test was considered for the experimental results with 95% concordance. The repeatability of the nano-assay was evaluated using the analysis of variance (ANOVA) comparison. The ROC curve was drawn in the SPSS software (IBM SPSS Statistics 23) to determine the assay sensitivity and specificity.

Results

Synthesis and characterization of different AuNPs

To prepare the biosensor, naked AuNPs were first synthesized using the citrate reduction method (15). The nanoparticles are stabilized and protected in the colloidal solution by the citrate layer that covers them. This coverage allows AuNPs to be kept sterile for several months (18). The size and charge of citrate-AuNPs were characterized by the DLS and zeta potential method. DLS analysis revealed a particle size distribution of ~18 nm (Figure 2e) and an average charge of -57.2 mV. TEM images of citrate-AuNPs confirmed the DLS results, and AuNPs morphology was observed to be uniform and spherical (Figure 2a). In addition, the UV-vis spectra of AuNPs showed an absorption peak at 518-520 nm (Figure 2d). This peak is caused by the surface plasmonic resonance of nanoparticles within the indicated size range. The colloidal molar concentration of AuNPs was determined to be 25 µM with ~2.946×10^{15} nanoparticles/mL. In this study, the nanoprobe and functionalized citrate-AuNPs were synthesized by attacking a thiol-linked poly-A

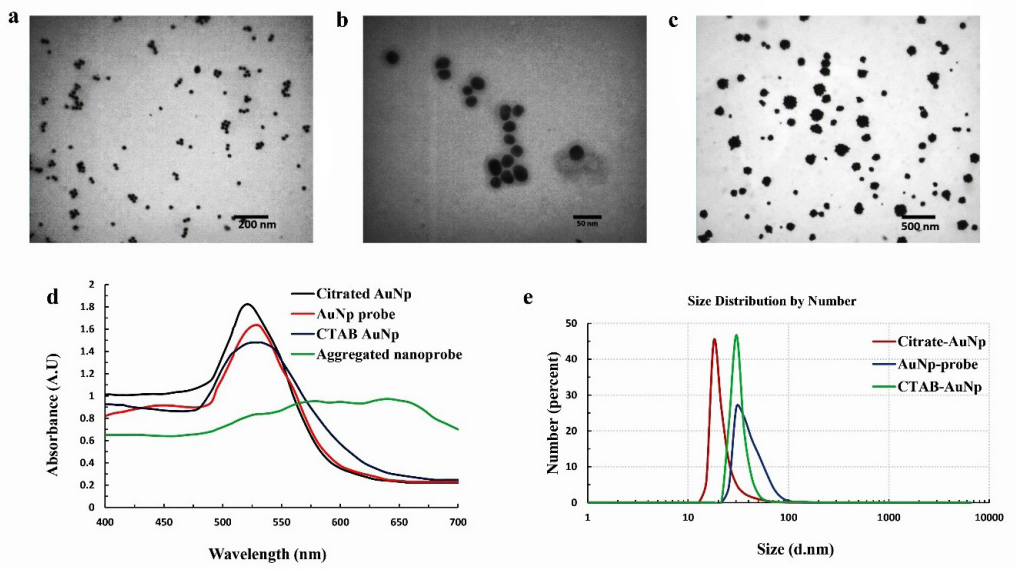

Figure 2. Characterization of different AuNPs. (a) Transmission electron microscopy (TEM) image of citrate-AuNPs, (b) AuNP-probes, (c) and CTAB-AuNPs. The image shows CTAB-AuNPs as groups of small AuNPs coated in a crust. (d) Spectroscopy of the citrate-AuNPs shows an absorption peak at 520 nm. The AuNP-probes exhibit a slight change and decrease in absorption peak to 525-530 nm due to functionalization. CTAB-AuNPs λ_{max} is 527 nm. The λ_{max} of the nanoprobe after CTAB-AuNPs-induced aggregation is shown by an increased peak (580-650 nm) and the absence of SPR. (e) The sizes of the citrate-AuNPs, AuNP-probe, and CTAB-AuNPs are 18 nm, 34.6 nm, and 29.3 nm, respectively. The increase in the nanoprobe's size confirms the functionalization of AuNPs.

oligonucleotide probe to the surface of the citrate-capped AuNPs. The thiol group has a stronger affinity for the gold surface than citrate, producing a strong covalent connection and providing high stability to the AuNP probes against cationic agents and aggregation (19). According to TEM analysis of HIV nanoprobe, citrate-AuNPs increased in size from 18 nm to 34.6 nm (Figures 2a and 2b), which is consistent with DLS analysis results (Figure 2e). In addition, zeta potential analysis showed a corresponding increase of surface charge from -57.2 mV to -61.3 mV. The increased size of the nanoprobe compared to AuNPs (16 nm) is a reason for the successful conjugation of the thiolated probe on the surface of AuNPs. Also, absorption spectrum analysis of the AuNP probes revealed a slight shift to λ_{max} at 525 nm versus the 520 nm peak of citrate-capped AuNPs (Figure 2d). This slight shift change can be due to the increase in the negative charge of nanoparticles following the binding of the probe to the citrate-AuNPs. These results suggest the proper binding of the probes to the surface of nanoparticles. TEM analysis revealed that the shape of CTAB-AuNPs have the same core/shell-like structure typical of numerous AuNPs coated within a shell (Figure 2c). The extinction spectra of CTAB-AuNPs displayed a clear peak at 526 nm, indicating the uniform distribution of spherical nanoparticles (Figure 2d).

Optimization of nano-assay conditions

The concentrations of the AuNP probes and the cationic agent greatly affect obtaining both false positive and false negative results. Typically, 120 probes for each 20 nm gold nanoparticle provide the best conditions for the stability of the nanoprobe against aggregation. Also, it provides an acceptable amount for hybridization with the target RNA.

In this study, the best probe concentration was determined by combining different concentrations of the TCEP-treated probe in the range of 0.5-150 µM with the citrate-AuNPs solution. This mixing was followed by a 16-hour incubation at 25 °C and the addition of CTAB-AuNPs solution. The results showed that the absorbance peak at 525 nm reached its maximum value at a probe concentration of 10 µM, suggesting that the probe had the greatest protective effect against CTAB-AuNPs-induced aggregation.

After performing the test with different CTAB-AuNP concentrations, the best result was obtained when the concentration of the CTAB-AuNPs was lower than the concentration of the AuNP-probes. As a result, in the current research, the optimal concentration of 10 µM probe for visual detection of color change was considered. Moreover, a 25-µM concentration of 18 nm AuNPs and 0.5 µM concentration of CTAB-AuNPs were considered.

The absorption of the RNA probes on the surface of the citrate-AuNPs can be affected by the pH of the reaction mixture, and the best absorption was seen at pH 7.0 (20). Therefore, nanoprobes synthesis and target RNA detection were performed in the proposed nano-assay at pH = 7.0. The temperature was another effective factor in performing a nano-assay. Since the target RNA is folded in the natural state, a high-temperature denaturation step for the target RNA-nanoprobes mixture was necessary to unfold the RNA tertiary structure. This step allows the probe access to the RNA molecules and their subsequent hybridization step. After denaturation and before adding the CTAB-AuNPs, a time interval at room temperature was required to refold the RNA and obtain its stable form (21).

Quantification of HIV-RNA in plasma using nano-assay

In this assay, the presence of the target HIV RNA and its binding to the AuNP probes is verified by a lack of color change in the reaction solution, in contrast to the negative control shifting to gray-blue. Depending on the target HIV RNA concentration, slight changes in the red color of the reaction solution were observed. A mixture containing HIV RNA exhibited high tolerance against induction by CTAB-AuNPs. Conversely, lower concentrations of the HIV target and negative samples diminished the electrostatic repulsion between nanoparticles. As a result, the cationic-AuNPs ionic strength prevailed and triggered nanoparticle aggregation and color change.

Solutions with high and low concentrations of the target RNA maintained their color with different intensities for several hours (12 hours). The lowest concentration of the target RNA (160 IU/mL), which was detectable quantitatively by nano-assay, was distinguishable from the negative control with the naked eye. In concentrations lower than 160 IU/mL, the change in mixture color was imperceptible to the naked eye. The highest reliable HIV RNA concentration determined by the standard curve was 1 500 000 IU/mL.

As the target RNA concentration increased, the height of the absorption peak of the AuNP-probes λ_{max} increased, indicating increased dispersion of nanoparticles in the mixture. However, in lower concentrations of the target RNA, the AuNP-probes λ_{max} shifted toward a higher wavelength (530 nm), and a shorter and wider λ_{max} peak was seen, which indicates aggregated nanoparticles (Figure 3d). A gradual color change was observed in the mixture with decreasing target concentration. Meanwhile, the HIV-negative sample mixture remained completely blue-grey due to the absence of the complementary sequence. This gradual color shift is directly related to the concentration of the HIV-RNA target (Figure 3d). Therefore, at high concentrations of the target RNA, the ratio of non-complex to complex nanoparticles is high. Furthermore, the opposite is seen in low concentrations of the target RNA and negative samples.

In this study, a standard curve was drawn to quantify nano-assay. All positive sample concentrations were determined using the standard curve (Figure 4b), ratio,

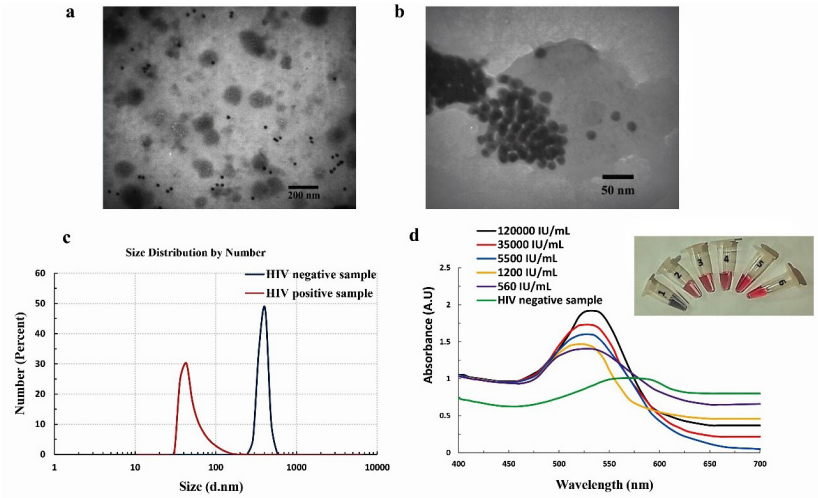

Figure 3. Characterization of AuNP-probes in the presence of HIV RNA and non-target RNA. (a) TEM image of the HIV-positive sample after colorimetric assay shows the dispersion of nanoparticles in the solution. (b) TEM images for HIV-negative samples show decreased inter-particle distance, which results in AuNPs aggregation. (c) An increase in nanoparticle size from 41.6 nm in positive samples to 355 nm in negative samples occurs due to the aggregation of AuNPs. (d) The UV/vis absorption spectra of the AuNPs solution in the presence of various concentrations of target HIV RNA and an HIV-negative sample (microtubes 1 to 6 containing an HIV-negative sample and HIV-positive samples with concentrations of 120,000 IU/mL, 35,000 IU/mL, 5,500 IU/mL, 1,200 IU/mL, and 560 IU/mL, respectively).

and equation previously mentioned. The absorbance peak and changes in the λ_{max} of the serial concentrations used to draw the standard curve are shown in Figure 4a. The plot demonstrated a linear relationship (Y=0.7456x-0.0203; R^2=0.974) between the ratio of A525/650 and the target RNA concentration. Also, a direct relationship was observed between the viral load and the intensity of the red color in the reaction solution. Moreover, plotting some positive samples at various concentrations on the standard curve (Figure S1) revealed a linear relationship (Y=0.8024x-0.211; R^2=0.968).

Following nano-assay quantification, the samples were all compared with the gold standard real-time RT-PCR technique (Table S1). The RT-qPCR identified 55 out of the 56 HIV samples as positive. On the other hand, the nano-assay identified 50 out of the 56 as positive, with a 95% concordance. The RT-qPCR identified all HIV-negative samples as negative. Meanwhile, three samples out of 38 HIV- negative cases were identified as positive cases by the nano-assay.

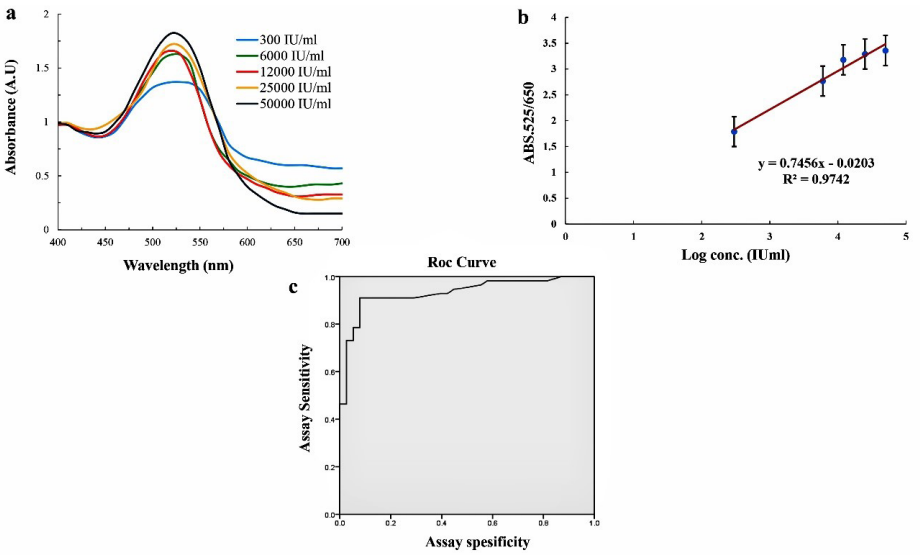

Figure 4. Quantification of HIV RNA in clinical plasma samples by the nano-assay. (a) The extinction spectra changes of samples with serial dilutions from 300 IU/mL up to 50,000 IU/mL. As the concentration decreases, the SPR (λ_{max}) decreases and shifts to a longer wavelength (580-650 nm) with a broader peak width. (b) The standard curve of serial dilutions shows that the ratio of A525/650 is a function of specific target concentration spiked in with increasing concentrations of the HIV RNA. The error bars represent the standard deviation of the mean of the three reactions. (c) The ROC curve was drawn by the SPSS 23 software; the sensitivity at the Y-axis was plotted against the specificity at the X-axis. The area under the ROC curve and standard error are 0.853 and 0.041, respectively.

According to the statistical analysis, the sensitivity, specificity, and accuracy of the nano-assay were determined as 89.2%, 92.1%, and 90.4%, respectively. The colorimetric nano-assay had a cut-off value of 1.59 (A525/A650) with a detection limit of 160 IU/mL. Values higher than the cut-off were considered positive. Also, the biosensor repeatability was assessed under identical conditions by three consecutive absorbance measurements (A525/A650) of the samples examined with nanoassay. The obtained suitable relative standard deviation (RSD) of 3.8% demonstrates the biosensor exhibits satisfactory repeatability. In addition, to evaluate the stability of the nanoprobe solution, the synthesized biosensor was stored at 4℃ and used to nanoassay once a day. After 30 days, the test's repeatability almost remained constant, with an RSD of <5%. This value confirms both the durability and satisfactory repeatability of the developed sensor for HIV-RNA detection.

Assessment of the charge and size of different nanoparticles and comparing RT-qPCR with nano-assay

Changes in both positive and negative HIV samples were assessed using TEM and DLS. HIV-positive samples had a negative charge resulting from the phosphate backbone of the attached RNA sequence to the AuNP probes. Conjugation of the target RNA to the nanoprobes and cationic-AuNPs distribution along and within the HIV-RNA strands causes resistance of nanoparticles to CTAB-AuNPs-induced aggregation (Figure 3a). Conversely, HIV-negative samples were positively charged indicating a reduction of the inter-particle distance and electrostatic force between AuNP-probes and the effect of CTAB-AuNPs on the environment of nanoparticles in the absence of the target RNA (Figure 3b) (22). Nanoparticles' size in HIV-positive samples increased slightly to 41.6 nm. This size growth can be due to the difference in the amount of non-dispersed to dispersed nanoparticles, which can change depending on the target concentration in the sample. The negative HIV sample images showed the increased size of nanoparticles to 355 nm due to the aggregation of the nanoparticles. Figure 5 presents a summary of the zeta potential and size of AuNPs and a comparison between the AuNP-based colorimetric assay and RT-qPCR.

Discussion

Lack of detectable antibodies and a transient high viral load without particular clinical signs characterize the early stage of HIV infection. As a result, using viral markers like HIV-1 RNA and DNA to identify infection status is considered the best detection method. However, employing PCR-based techniques to detect viral nucleic acids directly is highly technical and requires specialized personnel, equipment, and laboratory infrastructure (23).

Because their optical and electrical features are well-suited for chemical sensing and biolabeling, AuNPs have received much attention compared to other nanometals (24).

Compared to previous research (Table 1), in the present work, a simple, rapid, and cost-effective LSPR-colorimetric and ratiometric assay was developed using modified AuNPs to detect unamplified HIV RNA in clinical samples directly. In this assay, the aggregation of the nanoparticles resulted in a color change from red to blue that is easily detectable by the naked eye or UV-vis spectrometry. One

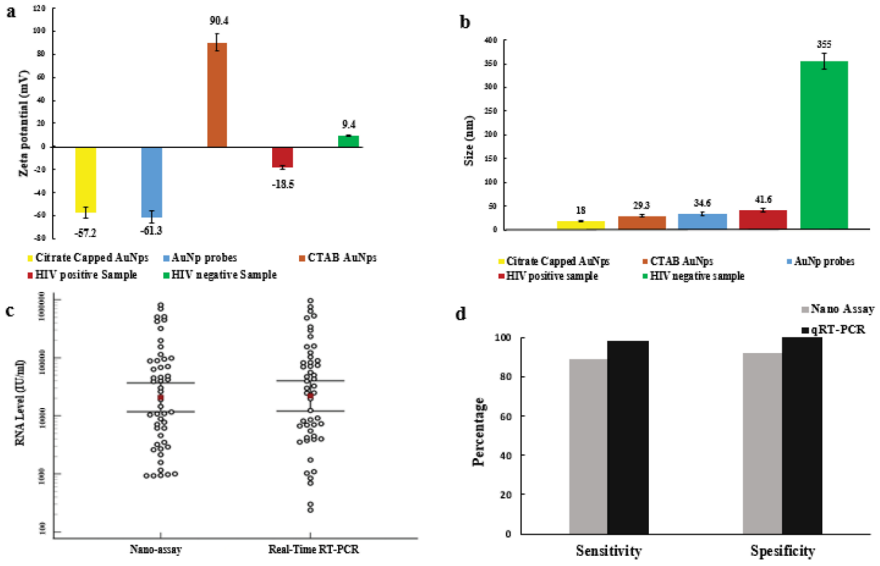

Figure 5. Changes in zeta potential and size of AuNPs and comparison of the colorimetric assay and RT-qPCR. (a) Charges of different AuNPs; the HIV-negative sample has a positive charge due to the coating of the nanoprobe with cationic AuNPs, while the HIV-positive samples keep their negative charge. (b) The diameter of the different AuNPs: an increase in AuNP size is seen in HIV-negative samples due to aggregation. (c) Comparison of mean viral load (IU/mL) and standard deviation in colorimetric method (104385.5 ± 26656) and RT-qPCR (114315.7 ± 29638) shows no significant difference. (d) The sensitivity and specificity of the nano-assay are 89.2% and 92.1%, respectively, in contrast to the RT-qPCR, which are 98.2% and 100%, respectively.

Table 1. A comparison between several techniques based on gold nanoparticles for viruses detection

Detection methods	Virus	Limit of detection	Reference
SPR (GNP-Antibody)	HIV	98 ± 39 copies/mL	(25)
SPR (GNP-based PC sensor)	HIV-1	10^4 to 10^8 copies/mL	(28)
LSPR (AuNP-dots-Antibody)	HIV-1	200 fg/mL	(29)
LSPR (AuNP core-SNAs)	HIV-1	1.5 pmol	(30)
Nanoparticle-based BCA assay	HIV-1	0.1-1 pg/mL	(31)
GLSS-PCR (GNP-Antibody)	HIV-1	106 copies/mL	(26)
DPN-fabricated nanoarray (GNP-Aptamer)	HIV-1	0.025 pg/mL	(27)
LSPR	Infeluenza (H1N1)	13.9 pg/mL	(32)
SPR	Infeluenza	0.5 μ	(33)
Optical	Hepatitis C	80 PM	(34)

of the disadvantages of previous methods compared to the current nano-assay is the identification of HIV infection based on antigen detection instead of nucleic acid (25-27). While the levels of anti-HIV IgM antibodies are low, the relatively wide linearity range discovered in this work will be helpful for the early identification of acute HIV infections. This wide range is especially beneficial when detecting the infection in the immunological window period. It will also help identify HIV infection in children born to mothers who have the disease and have maternal antibodies in their bloodstream.

In addition, the present NCL assay can be performed using one type of nanoprobe on total RNA and does not need DNA linker, cDNA synthesis and amplification (30). Additionally, the assay's turnaround time is considerably quicker than that of traditional detection techniques (less than 70 minutes, including RNA extraction). Unlike our work, unmodified AuNPs were used in previous research (31, 34), which is less sensitive. The explanation is that free probes have a greater tendency to bind to AuNPs in competition with the HIV target. In the present research, naked AuNPs were first synthesized using the citrate reduction method to prepare the biosensor. Next, the nanoparticles are stabilized and protected in the colloidal solution by the citrate layer. This layer covers them, allowing AuNPs to be kept sterile for several months (24). To modify citrate-AuNPs, a thiol-linked poly-A oligonucleotide was used here. The poly-A segments are used as spacers for organized immobilization. Poly-A tails dramatically increased the hybridization efficiency by reducing the steric barrier between certain probe sequences and the AuNP surface (35). Attachment of the probes to AuNPs produced particles that were stable and responsive to the intended analyte. The HIV AuNPs biosensor could be stored at 4℃ for 3 months without changing its integrity and analytical sensitivity (18). The significant advantage of this research is the use of modified AuNPs and the resulting improved sensitivity compared to unmodified AuNP assays, as free probes could be adsorbed onto AuNPs and decrease the assay's sensitivity (36).

In the case of positive samples, conjugation of the target RNA to the nanoprobes and dispersion of cationic nanoparticles along the RNA molecules make nanoprobes resist the aggregation induced by CTAB-AuNPs. Thus, the solution color remained red. To verify our theory, we took TEM images from a positive sample (Figure 3a). In the absence of HIV RNA, the CTAB-AuNPs reduce the inter-particle distances, leading to AuNPs aggregation and a change of color from red to blue (37). TEM images from negative samples revealed the aggregation of AuNPs (Figure 3b). In this study, HIV RNA was quantified using the nano-assay. To this end, a standard curve was generated, and the results were compared with RT-qPCR. A direct relationship was observed between the increase in the target concentration and the λ525/λ650 absorption ratio. Besides, a direct relationship was observed between the viral load and the intensity of the red color in the reaction solution. The assay had a DOL of 160 IU/mL, specificity of 92.1%, and sensitivity of 89.2%. The possibility of determining a cut-off value to differentiate between positive and negative samples in this nano-assay indicates its feasibility for routine diagnosis and easy interpretation of the results.

Moreover, the standard curve illustrated an acceptable linear absorption-load relationship in various virus loads. With further development and optimization, this method can be used to detect and quantify other RNA or DNA targets. The use of unamplified HIV RNA is another benefit of this assay. There are some drawbacks to PCR-based tests that could limit their application and hinder the reliability of results. These drawbacks include primer length constraints, non-specific amplification, primer dimers, contamination, the requirement for many temperature cycles, and the use of hazardous compounds. However, these shortcomings are absent in this nano-assay, where a fairly straightforward technique is employed

based on the color change of AuNPs and spectroscopy. Additionally, the assay's turnaround time is considerably quicker than that of traditional detection techniques (less than 70 minutes).

False positive and negative results may occur during nano-assay performance for various reasons. The attachment of too few probes to AuNPs leads to immediate aggregation of nanoparticles when adding the cationic agent even in the presence of the target RNA, resulting in false negative results. On the other hand, the final probe concentration of more than 10 µM created a steric hindrance on the surface of the AuNPs, which increased the possibility of false positive results (36). The use of cationic CTAB-AuNPs in this assay instead of conventional salts (NaCl and $MgCl_2$) led to a sensitivity improvement. Common monovalent or divalent cationic salts show a higher degree of nanoparticle aggregation due to their strong ionic strength, which ultimately increases the possibility of false negatives. Furthermore, in high concentrations of the CTAB-AuNPs, the aggregation of nanoparticles was observed even in the presence of the target RNA (false negative). This observation is probably due to the high positive charge of the cationic-AuNPs, owing to the presence of quaternary ammonium cations (38). It is of note that if the RNA was not denatured at high temperatures, the aggregation of nanoparticles and the color change of the solution would occur (false negative) immediately after adding the CTAB-AuNPs, even if the concentration of the target RNA was high. On the other hand, increasing the denaturation time may increase the possibility of non-specific binding of nucleic acids other than HIV-RNA to the nanoprobes (false positive) (21). To our knowledge, this is the first study on using modified gold nanoparticles and CTAB cationic nanoparticles for detecting unamplified HIV nucleic acid. Nevertheless, additional research is needed to improve the assay's sensitivity, specificity, and LOD.

Conclusion

Here, a novel, economical, and effective AuNPs-based quantitative colorimetric assay was developed as a promising approach to detect unamplified HIV RNA in clinical samples directly. This sequence-specific approach uses the inhibitory effect of the target RNA on nanoprobes assembly, thus preventing the plasmonic color change of AuNPs colloidal solution. The stability or aggregation of the nanoprobes relies on the cationic AuNPs and the target RNA. The nanoassay can confirm the presence of HIV-RNA within 70 min, both quantitatively using spectrophotometry and qualitatively by visual inspection. While the levels of anti-HIV IgM antibodies are low, the assay could detect HIV-1 RNA with a potential detection limit of 160 IU/mL, and the standard curve plot showed a relatively wide linear range that could be valuable for the early detection of acute HIV infection. To improve the assay's sensitivity, specificity, and LOD, we suggest investigating other cationic nanoparticles that induce aggregation of AuNPs. Also, the NCL process requires a larger amount of the target to prevent aggregation following the addition of a cationic agent. Therefore, increasing the initial plasma volume for RNA extraction can effectively improve the sensitivity. We anticipate that this established AuNPs-based method will provide rapid and accurate diagnostic results for epidemiological surveillance, especially in resource-limited settings, and could easily develop into commercial diagnostic kits and automated chips. Moreover, by creating and utilizing several particular probes, this nano-assay may be used to identify a variety of microorganisms.

Limitations of the study

No limitations were observed in this study.

Acknowledgments

The authors acknowledge the patients and coworkers who directly and indirectly assisted us in conducting this study and writing this publication.

Authors' contribution

Conceptualization: Maryam Fatemipour, Seyed Hamidreza Monavari and Masoumeh Zahmatkeshan.
Data curation: Mohammad Reza Rezvani, Maryam Fatemipour and Vahid Pirhajati Mahabadi.
Formal analysis: Behnam Khodadost, Seyed Ahmad Dehdast.
Funding acquisition: Seyed Hamidreza Monavari.
Investigation: Maryam Fatemipour, Seyed Hamidreza Monavari.
Methodology: Ahmad Tavakoli, Maryam Fatemipour.
Project administration: Seyed Hamidreza Monavari
Resources: Seyed Jalal Kiani, Farah Bokharaei-Salim.
Software: Behnam Khodadost, Seyed Ahmad Dehdast.
Supervision: Seyed Hamidreza Monavari, Masoumeh Zahmatkeshan.
Validation: Farah Bokharaei-Salim, Maryam Fatemipour.
Visualization: Maryam Fatemipour, Seyed Jalal Kiani and Vahid Pirhajati Mahabadi.
Writing–original draft: Milad Sabaei, Maryam Fatemipour, Seyed Hamidreza Monavari, Masoumeh Zahmatkeshan and Ahmad Tavakoli.
Writing–review & editing: All authors.

Conflicts of interest

The authors declare that they have no competing interests.

Ethical issues

The research conducted in this study adhered to the principles outlined in the Declaration of Helsinki and was approved by the Ethics Committee of Iran University of Medical Sciences (Ethical code# IR.IUMS.FMD. REC.1400.153). Accordingly, written informed consent was taken from all participants before any intervention. The study was registered in Research Registry IUMS (identifier: 20756). This study was extracted from Ph.D., thesis of Maryam Fatemipour at the department of medical virology of Iran University of Medical Sciences (Thesis #21 in the medical school). The authors have fully complied with ethical issues, such as plagiarism, data fabrication, and double publication.

Funding/Support

The Research Deputy of the Iran University of Medical Sciences

provided financial assistance for the current work (Grant #19545).

Supplementary files

Supplementary file 1 contains Figure 1 and Tables S1-S2.

References

1. Sundquist WI, Kräusslich HG. HIV-1 assembly, budding, and maturation. Cold Spring Harb Perspect Med. 2012;2:a006924. doi: 10.1101/cshperspect.a006924.
2. Fatin MF, Ruslinda AR, Md Arshad MK, Tee KK, Ayub RM, Hashim U, et al. HIV-1 Tat biosensor: Current development and trends for early detection strategies. Biosens Bioelectron. 2016;78:358-366. doi: 10.1016/j.bios.2015.11.067.
3. Kabir MA, Zilouchian H, Caputi M, Asghar W. Advances in HIV diagnosis and monitoring. Crit Rev Biotechnol. 2020;40:623-638. doi: 10.1080/07388551.2020.1751058.
4. Zhao WW, Han YM, Zhu YC, Zhang N, Xu JJ, Chen HY. DNA Labeling Generates a Unique Amplification Probe for Sensitive Photoelectrochemical Immunoassay of HIV-1 p24 Antigen. Anal Chem. 2015;87:5496-9. doi: 10.1021/acs.analchem.5b01360.
5. Jangam SR, Agarwal AK, Sur K, Kelso DM. A point-of-care PCR test for HIV-1 detection in resource-limited settings. Biosens Bioelectron. 2013;42:69-75. doi: 10.1016/j.bios.2012.10.024.
6. Kim EY, Stanton J, Korber BT, Krebs K, Bogdan D, Kunstman K, et al. Detection of HIV-1 p24 Gag in plasma by a nanoparticle-based bio-barcode-amplification method. Nanomedicine (Lond). 2008;3:293-303. doi: 10.2217/17435889.3.3.293.
7. Hurt CB, Nelson JAE, Hightow-Weidman LB, Miller WC. Selecting an HIV Test: A Narrative Review for Clinicians and Researchers. Sex Transm Dis. 2017;44:739-746. doi: 10.1097/OLQ.0000000000000719.
8. Rosi NL, Mirkin CA. Nanostructures in biodiagnostics. Chem Rev. 2005;105:1547-62. doi: 10.1021/cr030067f.
9. De Roe C, Courtoy PJ, Baudhuin P. A model of protein-colloidal gold interactions. J Histochem Cytochem. 1987;35:1191-8. doi: 10.1177/35.11.3655323.
10. Huang KS, Lin YC, Su KC, Chen HY. An electroporation microchip system for the transfection of zebrafish embryos using quantum dots and GFP genes for evaluation. Biomed Microdevices. 2007;9:761-8. doi: 10.1007/s10544-007-9087-x.
11. Elghanian R, Storhoff JJ, Mucic RC, Letsinger RL, Mirkin CA. Selective colorimetric detection of polynucleotides based on the distance-dependent optical properties of gold nanoparticles. Science. 1997;277:1078-81. doi: 10.1126/science.277.5329.1078.
12. Larguinho M, Canto R, Cordeiro M, Pedrosa P, Fortuna A, Vinhas R, et al. Gold nanoprobe-based non-crosslinking hybridization for molecular diagnostics. Expert Rev Mol Diagn. 2015;15:1355-68. doi: 10.1586/14737159.2015.1077704.
13. Sato K, Hosokawa K, Maeda M. Rapid aggregation of gold nanoparticles induced by non-cross-linking DNA hybridization. J Am Chem Soc. 2003;125:8102-3. doi: 10.1021/ja034876s.
14. Robinson DB, Buffleben GM, Langham ME, Zuckermann RN. Stabilization of nanoparticles under biological assembly conditions using peptoids. Biopolymers. 2011;96:669-78. doi: 10.1002/bip.21588.
15. Turkevich J, Stevenson PC, Hillier J. A study of the nucleation and growth processes in the synthesis of colloidal gold. Discussions of the Faraday Society. 1951;11:55-75. doi:10.1039/DF9511100055.
16. Hurst SJ, Lytton-Jean AK, Mirkin CA. Maximizing DNA loading on a range of gold nanoparticle sizes. Anal Chem. 2006;78:8313-8. doi: 10.1021/ac0613582.
17. Scarabelli L, Sánchez-Iglesias A, Pérez-Juste J, Liz-Marzán LM. A "Tips and Tricks" Practical Guide to the Synthesis of Gold Nanorods. J Phys Chem Lett. 2015;6:4270-9. doi: 10.1021/acs.jpclett.5b02123.
18. Hamdy ME, Del Carlo M, Hussein HA, Salah TA, El-Deeb AH, Emara MM, et al. Development of gold nanoparticles biosensor for ultrasensitive diagnosis of foot and mouth disease virus. J Nanobiotechnology. 2018;16:48. doi: 10.1186/s12951-018-0374-x.
19. Xue Y, Li X, Li H, Zhang W. Quantifying thiol-gold interactions towards the efficient strength control. Nat Commun. 2014;5:4348. doi: 10.1038/ncomms5348.
20. Ojea-Jiménez I, Puntes V. Instability of cationic gold nanoparticle bioconjugates: the role of citrate ions. J Am Chem Soc. 2009;131:13320-7. doi: 10.1021/ja902894s.
21. Doerrbecker J, Meuleman P, Kang J, Riebesehl N, Wilhelm C, Friesland M, et al. Thermostability of seven hepatitis C virus genotypes in vitro and in vivo. J Viral Hepat. 2013;20:478-85. doi: 10.1111/jvh.12055.
22. Fenger R, Fertitta E, Kirmse H, Thünemann AF, Rademann K. Size dependent catalysis with CTAB-stabilized gold nanoparticles. Phys Chem Chem Phys. 2012;14:9343-9. doi: 10.1039/c2cp40792b.
23. Sivapalasingam S, Essajee S, Nyambi PN, Itri V, Hanna B, Holzman R, et al. Human immunodeficiency virus (HIV) reverse transcriptase activity correlates with HIV RNA load: implications for resource-limited settings. J Clin Microbiol. 2005;43:3793-6. doi: 10.1128/JCM.43.8.3793-3796.2005.
24. Jain PK, Lee KS, El-Sayed IH, El-Sayed MA. Calculated absorption and scattering properties of gold nanoparticles of different size, shape, and composition: applications in biological imaging and biomedicine. J Phys Chem B. 2006;110:7238-48. doi: 10.1021/jp057170o.
25. Inci F, Tokel O, Wang S, Gurkan UA, Tasoglu S, Kuritzkes DR, et al. Nanoplasmonic quantitative detection of intact viruses from unprocessed whole blood. ACS Nano. 2013;7:4733-45. doi: 10.1021/nn3036232.
26. Tang J, Zhou L, Gao W, Cao X, Wang Y. Visual DNA microarrays for simultaneous detection of human immunodeficiency virus type-1 and Treponema pallidum coupled with multiplex asymmetric polymerase chain reaction. Diagn Microbiol Infect Dis. 2009;65:372-8. doi: 10.1016/j.diagmicrobio.2009.07.017.
27. Lee K-B, Kim E-Y, Mirkin CA, Wolinsky SM. The Use of Nanoarrays for Highly Sensitive and Selective Detection of Human Immunodeficiency Virus Type 1 in Plasma. Nano Letters. 2004;4:1869-72. doi:10.1021/nl049002y.
28. Shawky SM, Guirgis BS, Azzazy HM. Detection of unamplified HCV RNA in serum using a novel two metallic nanoparticle platform. Clin Chem Lab Med. 2014;52:565-72. doi: 10.1515/cclm-2013-0521.
29. Lee JH, Kim BC, Oh BK, Choi JW. Highly sensitive localized surface plasmon resonance immunosensor for label-free detection of HIV-1. Nanomedicine. 2013;9:1018-26. doi: 10.1016/j.nano.2013.03.005.
30. Zou L, Ling L. Ultrasensitive Detection of HIV DNA with Polymerase Chain Reaction-Dynamic Light Scattering. Anal Chem. 2018;90:13373-13377. doi: 10.1021/acs.analchem.8b03052.
31. Dong H, Liu J, Zhu H, Ou CY, Xing W, Qiu M, et al. Two types of nanoparticle-based bio-barcode amplification assays to detect HIV-1 p24 antigen. Virol J. 2012;9:180. doi: 10.1186/1743-422X-9-180.
32. Chang YF, Wang SF, Huang JC, Su LC, Yao L, Li YC, et al. Detection of swine-origin influenza A (H1N1) viruses using a localized surface plasmon coupled fluorescence fiber-optic biosensor. Biosens Bioelectron. 2010;26:1068-73. doi:

10.1016/j.bios.2010.08.060.
33. Nilsson CE, Abbas S, Bennemo M, Larsson A, Hämäläinen MD, Frostell-Karlsson A. A novel assay for influenza virus quantification using surface plasmon resonance. Vaccine. 2010;28:759-66. doi: 10.1016/j.vaccine.2009.10.070.
34. Griffin J, Singh AK, Senapati D, Lee E, Gaylor K, Jones-Boone J, et al. Sequence-specific HCV RNA quantification using the size-dependent nonlinear optical properties of gold nanoparticles. Small. 2009;5:839-45. doi: 10.1002/smll.200801334.
35. Singh A, Snyder S, Lee L, Johnston AP, Caruso F, Yingling YG. Effect of oligonucleotide length on the assembly of DNA materials: molecular dynamics simulations of layer-by-layer DNA films. Langmuir. 2010;26:17339-47. doi: 10.1021/la102762t.
36. Shawky SM, Bald D, Azzazy HM. Direct detection of unamplified hepatitis C virus RNA using unmodified gold nanoparticles. Clin Biochem. 2010;43:1163-8. doi: 10.1016/j.clinbiochem.2010.07.001.
37. Koyfman AY, Braun G, Magonov S, Chworos A, Reich NO, Jaeger L. Controlled spacing of cationic gold nanoparticles by nanocrown RNA. J Am Chem Soc. 2005;127:11886-7. doi: 10.1021/ja051144m.
38. Li H, Rothberg LJ. Label-free colorimetric detection of specific sequences in genomic DNA amplified by the polymerase chain reaction. J Am Chem Soc. 2004;126:10958-61. doi: 10.1021/ja048749n.